Xerogel Solvothermal in Different Alcohols of Cu and N Codoped TiO$_2$ Powders: Characterization Photocatalytic Oxidation of Acetone

Cui Ping LIU [1, 2], Tao YU [1] *, Xin TAN [1]

[1] *School of Chemical Engineering and Technology, Tianjin University, Tianjin 300072, China*
[2] *School of Science, Tianjin Chengjian University, Tianjin 300384, China*

In this study, mesoporous Cu and N co-doped TiO$_2$ crystals were synthesized with Cu and N co-doped titania xerogel by solvothermal treatment in different alcohols and the characteristics of Cu and N co-doped TiO$_2$ were investigated with XRD, SEM, UV-vis and N$_2$ sorption analysis. Results indicated that different alcohols facilitated formation and stability of pure anatase phase. The photocatalytic activity of samples was evaluated by the photocatalytic oxidation of acetone under visible light. The extraordinary photocatalytic performance of the Cu and N co-doped TiO$_2$ crystals were synthesized with titania xerogel by solvothermal treatment in ethyl alcohol. This enhanced photoactivity is related to the bandgap narrowing, good dispersibility, the smaller pores and the larger specific area.
Keywords: solvothermal, photocatalytic, acetone, alcohol.

1. INTRODUCTION

TiO$_2$ has been widely employed in water splitting, removal of wastes [1, 2], energy conversion/storage [3], photoanodes in dye sensitized cells [4, 5]. Metal doping and non-metal doping investigated as an effective method to improve the photocatalytic activity of TiO$_2$ [6, 7]. Recently, the photocatalytic activity of some Cu-N co-doped TiO$_2$ was considerably greater than that of the sample N doped TiO$_2$ and commercially available TiO$_2$, which is attributed to the synergistic effect of Cu-N co-doped. The sol-gel treatment was the major method to obtain nanosized Cu-N co-doped TiO$_2$ particles. Theoretical simulation work also found that Cu-N co-doping could broaden the absorption spectrum of anatase TiO$_2$ to the visible light region and increase its quantum efficiency [8, 9].

Typically, the xerogel of Cu-N co-doped TiO$_2$ obtained by sol-gel method are amorphous and require a subsequent thermal treatment that leads to crystallization. The calcination process often produces particle agglomeration and phase transformation. The solvothermal method is an alternative to calcination for promoting crystallization under mild temperatures [10, 11]. The high value of larger surface area, smaller particle size, and were more stable obtained by solvothermal method than those obtained by sol–gel methods [12, 13]. More importantly, solvothermal in alcohols can be used to well-defined sizes and geometric shapes due to smooth reaction and structural-direction of alcohols themselves. Usually, TiO$_2$ synthesized by solvothermal hydrolysis of different titanium precursors (TiF$_4$ or Ti(OC$_4$H$_9$)$_4$, etc) [14, 15]. However, there are few reports of TiO$_2$, which are prepared by xerogel solvothermal method. Also the different alcohol solvents effect on the formation and properties of TiO$_2$ particles was not studied by xerogel solvothermal method.

Against this background, we reported a facile route to prepare Cu-N co-doped TiO$_2$ with different alcohol solutions via xerogel solvothermal reaction. The fabrication process included hydrolysis of titanium precursor sol-gel transformation of the solution to xerogel, and further solvothermal treatment in different alcohols. The catalysts were characterized with XRD, SEM, UV-vis and BET. Photocatalytic oxidation acetone under visible light was investigated in this paper.

2. EXPERIMENT

At room temperature, a mixture solution of 1.0 mL nitric acid, 15 mL CH$_3$CH$_2$OH, 1.5 mL H$_2$O, 0.028 g copper nitrate(Cu(NO$_3$)$_2$·6H$_2$O) and 0.648 g urea, was dropped into the solution of 8.5 mL tetrabutyl titanate and 35 mL ethanol under magnetic stirrer. The doping amount of N and Cu were 4 wt.% and 0.6 wt.%. After stirred for 60 min, a gel was formed, then colloid was first dried at 80 °C to form xerogel. The xerogel was then added into the 30.0 mL different alcohol solutions, and the final solution was stirred for 0.5 h before being introduced into a 50 mL Teflon stainless steel autoclave. The autoclave was maintained at 120 °C for 12 h. The product washed by water and ethanol several times and dried at 80°C in oven. The Cu and N co-doped TiO$_2$ samples by solvothermal in ethyl alcohol, isopropyl alcohol and n-butyl alcohol were assigned as Cu$_{0.6}$N$_4$Ti-Et, Cu$_{0.6}$N$_4$Ti-Pr and Cu$_{0.6}$N$_4$Ti-Bu, respectively.

The crystalline phase of particles was determined using X-ray diffraction (Cu Kα radiation). Scherer's equation was used to calculate the particle size of titanium. Scanning electron microscope (SEM) images were obtained on a S-4800 electron microscope. The specific surface area (S_{BET}) was determined using NOVA-2000E according to the BET method. Barrette Joynere Halenda approach was used to calculate pore size distribution of the samples using the desorption data. UV-vis diffuse

---

* Corresponding author. Tel.: +0086-022-23503251; fax: +0086-022-23503215. E-mail address: *yutao@tju.edu.cn* (T. Yu)

reflectance spectra (DRS) were measured on UV-3600 UV-vis apparatus, using $BaSO_4$ as reference.

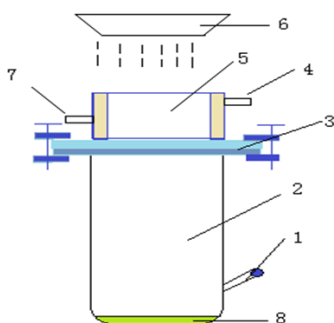The schematic of the photocatalytic reaction system is illustrated in Fig. 1.

Fig. 1. Experimental setup for photodegradation of gaseous acetone: 1 – sampling port; 2 – photoreductor; 3 – sealing; 4 – water oulet; 5 – cooling water; 6 – Xe lamp; 7 – water inlet; 8 – catalyst sample

Scanning electron microscope (SEM) images were obtained on a S-4800 electron microscope. The specific surface area (S_{BET}) was determined using NOVA-2000E according to the BET method. Barrette Joynere Halenda approach was used to calculate pore size distribution of the samples using the desorption data. UV-vis diffuse reflectance spectra (DRS) were measured on UV-3600 UV-vis apparatus, using $BaSO_4$ as reference.

The schematic of the photocatalytic reaction system is illustrated in Fig. 1. Photocatalytic oxidation of acetone was performed in a 300 mL cylindrical glass vessel with a Xe lamp as light source ($\lambda > 420$ nm). The sample powder was placed at the bottom center of the reactor, the gas valves on both sides of reactor were closed to seal the reactor. The acetone gas was then injected the cylindrical photoreactor. Then the reactor was kept in dark for 40 min to reach the adsorption equilibrium. After that, the visible light source was turned on and the inside temperature of the reactor was kept with circulation water. The acetone concentration was evaluated using gas chromato-graphy(GC-2014, Shimadzu,Tokyo) regularly.

3. RESULTS AND DISCUSSION

3.1. Characterization

Fig. 2 shows the XRD patterns for the powders synthesized in three different alcohols. On the same hydrothermal treatment conditions, $Cu_{0.6}N_4Ti$-Et, $Cu_{0.6}$-Ti-Pr and $Cu_{0.6}N_4Ti$-Bu showed different degrees of peak
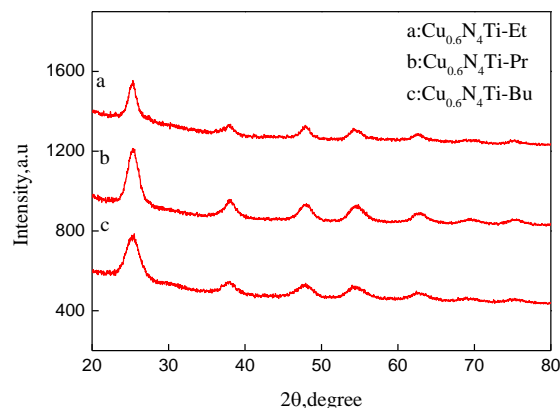
broadening ascribed to the varied crystallite size.

Fig. 2. XRD of the as-prepared $Cu_{0.6}N_4/TiO_2$ in different alcohols

Table 1. Textural characteristics of the as-prepared $Cu_{0.6}N_4/TiO_2$ in different alcohols

Sample	S_{BET}, m²/g	Pore volume, cm³/g	Pore diameter, nm
$Cu_{0.6}N_4Ti$-Et	188.38	0.06	3.38
$Cu_{0.6}N_4Ti$-Pr	178.06	0.15	3.84
$Cu_{0.6}N_4Ti$-Bu	162.29	0.14	3.80

The peak intensity of the $Cu_{0.6}N_4Ti$-Pr and $Cu_{0.6}N_4Ti$-Bu were broader than that of the $Cu_{0.6}N_4Ti$-Et sample. Generally, the crystalline domain size decreases with increasing line broadening. According to Scherer's equation, the particle sizes of $Cu_{0.6}N_4Ti$-Et, $Cu_{0.6}N_4Ti$-Pr and $Cu_{0.6}N_4Ti$-Bu are 6.1 nm, 5.4 nm and 4.8 nm, respectively. The particle size of sample $Cu_{0.6}N_4Ti$-Et is bigger than that of $Cu_{0.6}N_4Ti$-Pr and $Cu_{0.6}N_4Ti$-Bu. It demonstrated the crystallite size of reaction solvent with longer carbon chain suppressing the growth rate [16].

To obtain information about morphologies of $Cu_{0.6}N_4Ti$-Et, $Cu_{0.6}N_4Ti$-Pr $Cu_{0.6}N_4Ti$-Bu samples, some selected powders were investigated by scanning electron microscopy as shown in Fig. 3. As can be seen from the micrographs, most of the particles are highly agglomerated. The powders agglomerates (Fig. 3 b and c) can be as large as 1 μm. Whereas, the sample prepared through solvothermal by ethyl alcohol, agglomerates break to the smaller individual particles (Fig. 3 a). It can be seen that solvothermal by ethanol solvent, Cu and N co-doped TiO_2 provokes faster grains growth.
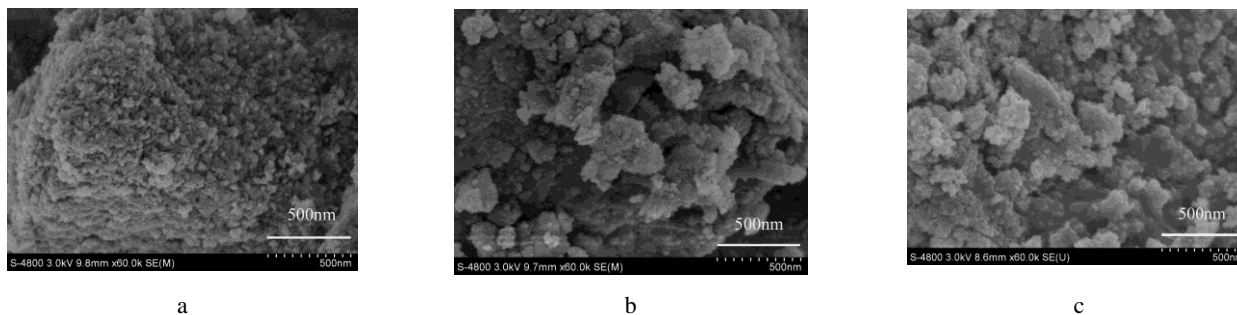

a   b   c

Fig. 3. SEM images of the as-prepared $Cu_{0.6}N_4/TiO_2$ in different alcohols: a – $Cu_{0.6}N_4Ti$-Et; b – $Cu_{0.6}N_4Ti$-Pr; c – $Cu_{0.6}N_4Ti$-Bu

The mesostructure characteristics of the as-prepared catalysts were also studied by nitrogen sorption measurements. The isotherms of materials of $Cu_{0.6}N_4Ti$-Et, $Cu_{0.6}N_4Ti$-Pr and $Cu_{0.6}N_4Ti$-Bu in Fig. 4 a exhibit type-IV behavior, which is characteristic of mesoporous materials based on the IUPAC classification [17].
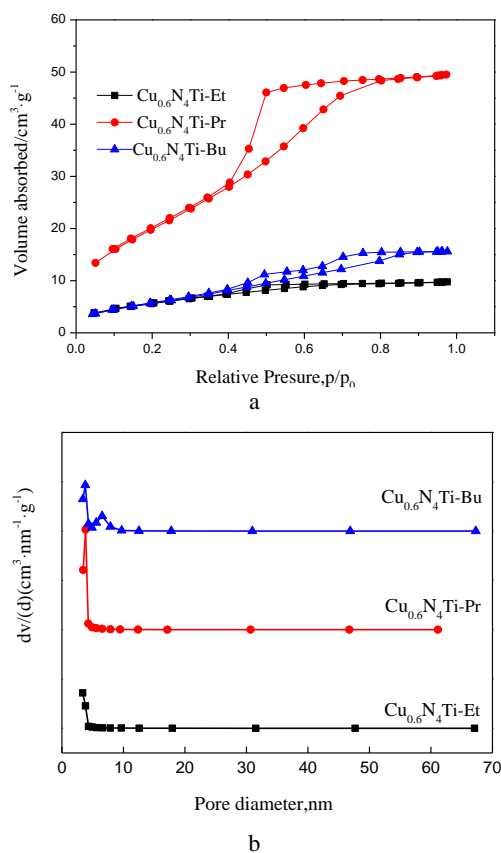

Fig. 4. a – nitrogen adsorption/desorption isotherms; b – pore size distributions of the as-prepared $Cu_{0.6}N_4/TiO_2$ in different alcohols

The type-IV isotherm of $Cu_{0.6}N_4Ti$-Pr and $Cu_{0.6}N_4Ti$-Bu are acknowledged in Fig. 4 a along with a hysteresis loop of type H2 characterizes, similar to that of $Cu_{0.6}N_4Ti$-Et, indicating ink-bottle-shaped pores.

Table 1 also shows quantitative details on BET surface area, pore volume and average pore size of $Cu_{0.6}N_4Ti$–Et, $Cu_{0.6}N_4Ti$-Pr and $Cu_{0.6}N_4Ti$-Bu. The hydro-thermal by different alcohols changed the surface area unobviously, but pore volume increased from $0.06 – 0.15$ cm^3/g. It can be seen that among the $Cu_{0.6}N_4Ti$–Et, $Cu_{0.6}N_4Ti$-Pr and $Cu_{0.6}N_4$-Ti-Bu, $Cu_{0.6}N_4Ti$-Et exhibited largest BET surface area, smallest pore volume and pore size. These results indicated that the surface area of the $Cu_{0.6}N_4Ti$-Et catalyst is highly enhanced, due to the formation of small pores; and the catalyst would keep more space between the particles, and avoid the collapse of microspores [18]. The smaller pores and the larger specific surface area of the TiO$_2$ samples are favorable to the photocatalytic degradation [19]. However, it is interesting to note that the surface area of $Cu_{0.6}N_4Ti$-Et (188.38 m^2/g) is bigger than that of $Cu_{0.6}N_4Ti$-Pr (178.06 m^2/g) and $Cu_{0.6}N_4Ti$-Bu(162.29 m^2/g) though the particle size of $Cu_{0.6}N_4Ti$-Et is much larger than that of $Cu_{0.6}N_4Ti$-Pr and $Cu_{0.6}N_4$ Ti-Bu, which indicates sample $Cu_{0.6}N_4Ti$-Pr and $Cu_{0.6}N_4$ Ti-Bu

have more amorphous structure according the XRD result [20].

The BJH analyses of the samples in Fig. 4 b exhibit similar pore size distributions patterns in spite of different solvents. Fig. 4 b displays narrow pore size distribution ($3 – 6$ nm) in the $Cu_{0.6}N_4Ti$-Et, $Cu_{0.6}N_4Ti$-Pr and $Cu_{0.6}N_4Ti$-Bu sample, which is indicative of a typical mesoporous material [21]. In particular, $Cu_{0.6}N_4Ti$-Bu shows double pore size distribution, one narrow peak in the range of $3 – 5$ nm and one broad distribution at $5 – 8$ nm. The hierarchical structure is favorable for dye molecules to access the pores [22].

Fig. 5 shows the UV-vis diffuse reflectance spectra of $Cu_{0.6}N_4Ti$-Et, $Cu_{0.6}N_4Ti$-Pr and $Cu_{0.6}N_4Ti$-Bu. The UV-vis DRS results indicate that $Cu_{0.6}N_4Ti$-Et are more sensitive to the visible light than $Cu_{0.6}N_4Ti$-Pr and $Cu_{0.6}N_4Ti$-Bu samples.
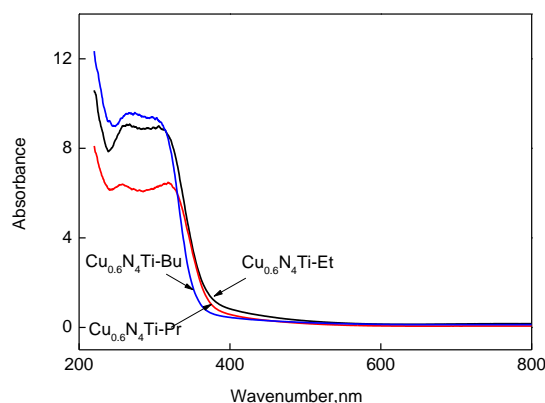
Fig. 5. UV-vis diffuse reflection spectra of $Cu_{0.6}N_4Ti$-Et, $Cu_{0.6}N_4Ti$-Pr and $Cu_{0.6}N_4Ti$-Bu

Kubelka-Munk function was used to estimate the bandgap energy of all samples. The calculated results showed that the bandgap of $Cu_{0.6}N_4Ti$-Et, $Cu_{0.6}N_4Ti$-Pr and $Cu_{0.6}N_4Ti$-Bu are 2.95 eV, 3.0 eV and 3.30 eV. The bandgap in a semiconductor material is closely related to the wavelength range absorbed, where the bandgap decreases with increasing absorption wavelength. The $Cu_{0.6}N_4Ti$-Et sample could be excited to produce more electron-hole pairs than $Cu_{0.6}N_4Ti$-Pr and $Cu_{0.6}N_4Ti$-Bu, which could result in higher photocatalytic activities. It is believed that the solvothermal modification by ethanol alcohol reduced the bandgap of the $Cu_{0.6}N_4TiO_2$ semiconductor significantly, which resulted in better photo-activity under visible light illumination.

3.2. Activity evaluation and kinetics of photocatalytic process analysis

Acetone is a common chemical used in industry. Photocatalytic oxidation of acetone was employed as a probe reaction to investigate the activities of as-synthesized TiO$_2$ under the irradiation of visible light ($\lambda > 420$ nm). As shown in Fig. 6 a, $Cu_{0.6}N_4Ti$-Et exhibits excellent photocatalytic activity, and can degrade 79 % acetone within 50 min, whereas 50 % and 45 % of acetone is degraded with $Cu_{0.6}N_4Ti$-Bu and $Cu_{0.6}N_4Ti$-Pr. During 30 min dark adsorption, 46 %, 3 % and 3 % of acetone was adsorbed on the surface of samples, respectively, which is beneficial for enhancing their photocatalytic activity.

In order to eliminate the adsorption effect, the pseudo-first order model was applied to the evaluation of the degradation rate. The model can be articulated by the equation below:

$$\ln(C_0/C)=kt, \qquad (1)$$

where k is the rate constant for pseudo-first-order reaction, C_0 is the initial concentration of the targeted contaminant (mg/L) and C is the final concentration of the targeted contaminant (mg/L). As shown in Fig. 6 b, the k value of $Cu_{0.6}N_4TiO_2$ sample prepared with the assistance of ethyl alcohol is 0.023 min^{-1}, which is larger than that prepared with the assistance of isopropyl alcohol and n-butyl alcohol. Cu and N co-doped TiO_2 nanoparticles modified by solvent of ethyl alcohol obviously enhanced the photocatalytic activity under visible light. $Cu_{0.6}N_4Ti$-Et exhibited a relatively highest photocatalytic performance due to the most efficient bandgap narrowing, the smaller pores and the larger specific surface of $Cu_{0.6}N_4Ti$-Et.

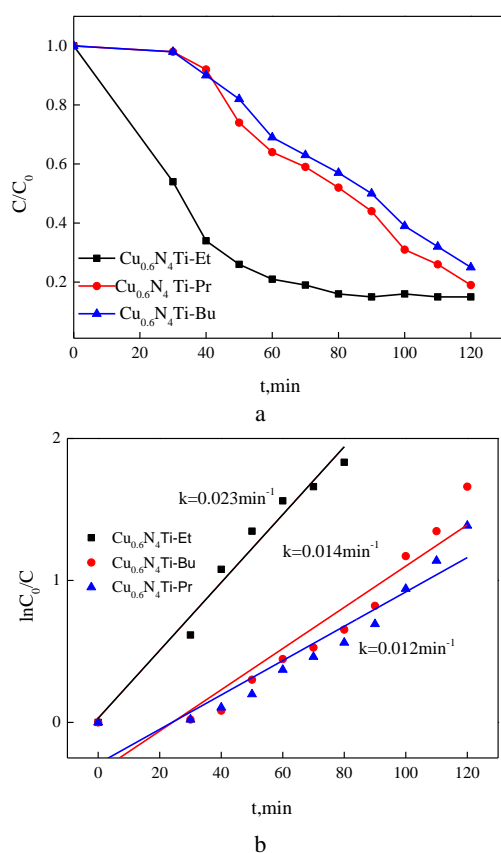**Fig. 6.** a – photocatalytic oxidation of acetone under visible light for $Cu_{0.6}N_4Ti$–Et, $Cu_{0.6}N_4Ti$–Pr and $Cu_{0.6}N_4Ti$–Bu; b – apparent rate constant (k) for photodegradation of acetone for $Cu_{0.6}N_4$ Ti–Et, $Cu_{0.6}N_4Ti$–Pr and $Cu_{0.6}N_4Ti$–Bu

Additionally, good dispersibility of $Cu_{0.6}N_4Ti$-Et is very advantageous in enhancing their photocatalysis efficiency. It is well known that crystalline and smaller size of particles showed higher catalytic activity. From the result of XRD, although the sizes of $Cu_{0.6}N_4Ti$-Bu and $Cu_{0.6}N_4Ti$-Pr were smaller than $Cu_{0.6}N_4Ti$-Et, $Cu_{0.6}N_4Ti$-Buand $Cu_{0.6}N_4Ti$-Pr showed lower catalytic activity. This phenomenon probably results from low crystallization of

$Cu_{0.6}N_4Ti$-Bu and $Cu_{0.6}N_4Ti$-Pr. As shown in Fig. 2, the peak intensity of XRD for $Cu_{0.6}N_4Ti$-Bu and $Cu_{0.6}N_4Ti$-Pr are weaker than $Cu_{0.6}N_4Ti$-Et.

4. CONCLUSIONS

This work developed a new approach to synthesize anatase Cu and N co-doped TiO_2 nanocrystals by xerogel solvothermal in different alcohols. After carefully characterizing the materials, we found that ethyl alcohol can result in a confined growth of well-crystalline and pure anatase particle. Ethanol alcohol reduced the bandgap of the Cu and N co-doped TiO_2 semiconductor. Ethanol alcohol highly enhanced the surface area of the Cu and N co-doped TiO_2 catalyst. The Cu and N co-doped TiO_2 prepared by ethanol alcohol showed good dispersibility than other alcohols. The Cu and N co-doped TiO_2 obtained by ethyl alcohol showed the highest photocatalytic oxidation of acetone under visible light due to the bandgap narrowing, good dispersibility, the smaller pores and the larger specific area.

REFERENCES

1. **Wong, C.L., Tan, Y.N., Mohamed, A.R.** A Review on the Formation of Titania Nanotube Photocatalysts by Hydrothermal Treatment *Journal of Environment Management* 92 2011: pp. 1669 – 1680. https://doi.org/10.1016/j.jenvman.2011.03.006

2. **Wold, A.** Photocatalytic Properties of TiO_2 *Chemical Materials* 5 1993: pp. 280 – 283. https://doi.org/10.1021/cm00027a008

3. **Zhao, Z., Sun, Z., Zhao, H.** Phase Control of Hierarchically Structured Mesoporous Anatase TiO_2 Microspheres Covered with {001} Facets *Journal of Materials Chemistry* 22 2012: pp. 21965 – 21971. https://doi.org/10.1039/c2jm35045a

4. **He, Z.M., Liu, J., Miao, J.W.** A One-pot Solvothermal Synthesis of Hierarchical Microspheres with Radially Assemble Single Crystalline TiO_2-nanorods for High Performance Dye-sensitized Solar Cells *Journal of Materials Chemistry C* 2 2014: pp. 1381 – 1385. https://doi.org/10.1039/c3tc32061h

5. **Rui, Y., Li, Y., Zhang, Q.** Facile Synthesis of Rutile TiO_2 Nanorod Microspheres for Enhancing Light-harvesting of Dye-sensitized Solar Cell *CrystEngComm* 15 2013: pp. 1651 – 1656. https://doi.org/10.1039/c2ce26691a

6. **Gombac, V., De, R.L., Gasparotto, A.** TiO_2 Nanopowders Doped with Boron and Nitrogen for Photocatalytic Applications *Chemical Physics* 339 2007: pp. 111 – 123. https://doi.org/10.1016/j.chemphys.2007.05.024

7. **Nasir, M., Lei, J.Y., Iqbal, W.** Study of Synergistic Effect of Sc and C Codoping on the Enhancement of Visible Light Photocatalytic Activity of TiO_2 *Applied Surface Science* 364 2016: pp. 446 – 454. https://doi.org/10.1016/j.apsusc.2015.12.166

8. **Song, K.X., Zhou, J.H., Bao, J.C.** Photocatalytic Activity of (Copper,Nitrogen) Codoped Titanium Dioxide Nanoparticles *Journal of the American Ceramic Society* 91 (4) 2008: pp. 1369 – 1371.
https://doi.org/10.1111/j.1551-2916.2008.02291.x

9. **Kim, C.S., Shin, J.W., Cho, Y.H.** Synthesis and Characterization of Cu/N Doped Mesoporous TiO_2 Visible Light Photocatalysts *Applied Catalysis A: General* 455 2013: pp. 211 – 218.
https://doi.org/10.1016/j.apcata.2013.01.041

10. **Yang, P., Ku, C., Hua, N., Du, Y.** Titanium Dioxide Nano-Particles Co-doped with Fe^{3+} and Eu^{3+} Ions for Photocatalysis *Materials Letter* 57 2002: pp. 794 – 801.
https://doi.org/10.1016/S0167-577X(02)00875-3

11. **Su, C., Hong, B.Y., Tseng, C.M.** Sol–gel Preparation and Photocatalysis of Titanium Dioxide *Catal Today* 96 2004: pp. 119 – 126.
https://doi.org/10.1016/ j.cattod.2004.06.132

12. **Wang, C.C.,Ying, J.Y.** Sol-gel Synthesis and Hydro-thermal Processing of Anatase and Rutile Titania Nanocrystals *Journal of Materials Chemistry* 11 1999: pp. 3113 – 3120.
https://doi.org/10.1021/cm990180f

13. **Zhou, W.J., Liu, X.Y., Cui, J.J.** Control Synthesis of Rutile TiO_2 Microspheres, Nanoflowers, Nanotrees and Nanobelts via Acid-hydrothermal Method and Their Optical Properties *Crystal Engineer Communication* 13 2011: pp. 4557 – 4663.
https://doi.org/10.1039/c1ce05186e

14. **Zhu, J., Wang, S.H., Bian, Z.F.** Solvothermally Controllable Synthesis of Anatase TiO_2 Nanocrystals with Dominant {001} Facets and Enhanced Photocatalytic Activity *CrystEngComm* 12 2010: pp. 2219 – 2224.
https://doi.org/10.1039/c000128g

15. **Zhou, J., Zhao, G.L., Song, B.** Solvent-controlled Synthesis of Three-dimensional TiO_2 Nanostructures via a One-step Solvothermal Route *CrystEngComm* 13 2011: pp. 2294 – 2302.
https://doi.org/10.1039/c0ce00793e

16. **Sakai, H., Kawahara, M., Shimazaki, M.** Preparation of Ultrafine Titanium Dioxide Particles Using Hydrolysis and Condensation Reactions in the Inner Aqueous Phase of Reversed Micelles: Effect of Alcohol Addition *Langmuir* 14 1998: pp. 2208 – 2212.
https://doi.org/10.1021/la970952r

17. **Gopal, M., Chan, W.J.M., De Jonghe, L.C.** Room Temperature Synthesis of Crystalline Metal Oxides *Journal of Materials Science* 32 1997: pp. 6001 – 6008.
https://doi.org/10.1023/A:1018671212890

18. **Gu, T., Jin, R., Liu, Y.** Promoting Effect of Calcium Doping on the Performances of MnO_x/TiO_2 Catalysts for NO Reduction with NH_3 at Low Temperature *Applied Catalyst B* 129 2013: pp. 30 – 38.
https://doi.org/10.1016/j.apcatb.2012.09.003

19. **Qu, Y.Z., Yao, M.M., Li, F.** Microstructures and Photocatalytic Properties of Fe^{3+}/Ce^{3+} Codoped Nanocrystalline TiO_2 Films *Water Air and Soil Pollution* 221 2011: pp. 13 – 21.
https://doi.org/10.1007/s11270-011-0765-1

20. **Liu, J., Zhao, Y., Shi, L.Y.** Solvothermal Synthesis of Crystalline Phase and Shape Controlled Sn^{4+}-doped TiO_2 Nanocrystals: Effects of Reaction Solvent *Applied Materials Interfaces* 3 2011: pp. 1261 – 1268.
https://doi.org/10.1021/am2000642

21. **Wang, C., Li, Q., Wang, R.D.** Synthesis and Characterization of Mesoporous TiO_2 with Anatase Wall *Materials Letter* 58 2004: pp. 1424 – 1426.
https://doi.org/10.1016/j.matlet.2003.10.006

22. **Yang, G.D., Wang, T., Yang, B.** Enhanced Visible-light Activity of F-N Co-doped TiO_2 Nanocrystals via Nonmetal Impurity, Ti^{3+} Ions and Oxygen Vacancies *Applied Surface Science* 287 2013: pp. 135 – 142.
https://doi.org/10.1016/j.apsusc.2013.09.094